The desmin network is a determinant of the cytoplasmic stiffness of myoblasts

Elisabeth Charrier[1,2,3], Lorraine Montel[1,4,5,6], Atef Asnacios[1], Florence Delort[2], Patrick Vicart[2], François Gallet[1], Sabrina Batonnet-Pichon[2], Sylvie Hénon[1]

[1] Univ Paris Diderot, CNRS, Matière et Systèmes Complexes UMR 7057, F-75013 Paris, France.

[2] Univ Paris Diderot, CNRS, Unité de Biologie Fonctionnelle et Adaptative, UMR 8251, F-75013 Paris, France.

[3] Institute for Medicine and Engineering, University of Pennsylvania, Philadelphia, Pennsylvania, USA.

[4] École Normale Supérieure, PSL Research University, Département de Chimie, F-75005 Paris, France

[5] Sorbonne Universités, UPMC Univ. Paris 06, PASTEUR, F-75005 Paris, France

[6] CNRS, UMR 8640 PASTEUR, F-75005 Paris, France

Keywords: intermediate filaments, cell rheology, myofibrillar myopathy, desmin, cytoskeleton

Corresponding author: Elisabeth Charrier,
Institute for Medicine and Engineering
University of Pennsylvania
1010 Vagelos Research Labs
3340 Smith Walk
Philadelphia, PA 19104-6393
Email: charrier@mail.med.upenn.edu
Tel: 215-260-6201
Fax: 215-573-6815

ABSTRACT

Background Information

The mechanical properties of cells are essential to maintain their proper functions, and mainly rely on their cytoskeleton. A lot of attention has been paid to actin filaments, demonstrating their central role in the cells mechanical properties, but much less is known about the participation of intermediate filament networks. Indeed the contribution of IFs, such as vimentin, keratins, and lamins, to cell mechanics has only been assessed recently. We study here the involvement of desmin, an intermediate filament specifically expressed in muscle cells, in the rheology of immature muscle cells. Desmin can carry mutations responsible for a class of muscle pathologies named desminopathies.

Results

In this study, using 3 types of cell rheometers, we assess the consequences of expressing wild-type or mutated desmin on the rheological properties of single myoblasts. We find that the mechanical properties of the cell cortex are not correlated to the quantity, nor the quality of desmin expressed. On the contrary, the overall cell stiffness increases when the amount of wild-type or mutated desmin polymerized in cytoplasmic networks increases. However, myoblasts become softer when the desmin network is partially depleted by the formation of aggregates induced by the expression of a desmin mutant.

Conclusions

We demonstrate that desmin plays a negligible role in the mechanical properties of the cell cortex but is a determinant of the overall cell stiffness. More particularly, desmin participates to the cytoplasm visco-elasticity.

Significance

Desminopathies are associated with muscular weaknesses attributed to a disorganization of the structure of striated muscle that impairs the active force generation. The present study evidences for the first time the key role of desmin in the rheological properties of myoblasts, raising the hypothesis that desmin mutations could also alter the passive mechanical properties of muscles, thus participating to the lack of force build up in muscle tissue.

INTRODUCTION

The cytoskeleton is recognized as the determinant of cell mechanical properties and the actin network has been evidenced as the key player due to its involvement in migration, differentiation and signaling pathways associated with the transduction of mechanical information (Asparuhova et al., 2009; Blanchoin et al., 2014; Ingber, 2006; Roca-Cusachs et al., 2013; Wang et al., 2009; Welch et al., 1997). However, it has been shown that intermediate filaments (IFs) also play a role in these cellular processes (Alam et al., 2011; Eckes et al., 1998; Ivaska et al., 2007, Homberg et al., 2015, Leduc et al. 2017) and that they participate in cell mechanics properties (Charrier et al., 2016; Charrier and Janmey, 2016; Guo et al., 2013; Seltmann et al., 2013, Ramms et al. 2013, Wang and Stamenović, 2000). Intermediate filaments are a class of proteins with a tripartite structure: hydrophilic head and tail, and a alpha-helical domain composed of hydrophilic and hydrophobic amino acids in the central position (Fuchs and Weber, 1994; Weber and Geisler, 1985). This particular structure allows the protein monomers to assemble (Chernyatina et al., 2012; Steinert et al., 1981) and to ultimately form networks within cells. IFs are organized into 6 classes depending on their function and expression profile. We are interested in the third class of IFs, which contains 4 proteins, including two homologous ones: desmin and vimentin, both cytoplasmic IFs, respectively expressed in muscular and mesenchymal cells. Our study focuses on desmin. Mutations in the gene encoding this protein lead to desminopathies, a class of rare genetic diseases belonging to the group of myofibrillar myopathies (Goldfarb et al., 2008). Patients with desminopathies suffer from alterations of their striated muscles, manifested clinically by muscular weaknesses and cardiomyopathies (Clemen et al., 2013). We focus here on the E413K mutation of desmin, a point mutation located at the beginning of the C-terminal domain of the protein that disturbs its assembly into filaments *in vitro* (Bär et al., 2007; Levin et al., 2010), and leads to skeletal muscle weakness in patients (Pruszczyk et al., 2007). We have recently shown that the expression of E413K mutated desmin *in cellulo* at the early stage of myoblasts alters these cells ability to generate traction forces (Charrier et al., 2016). We question here the impact of this mutation on the viscoelastic properties of myoblasts. A classical way to try and unravel the function of a protein is to look at the consequences of reducing its expression level with a knock down or suppressing it with a knock out. This approach has been used in past studies to characterize the implication of vimentin in cell mechanics (Eckes et al., 1998; Guo et al., 2013). A complementary approach is to study the impact of overexpressing the wild-type protein or a mutant. This is of particular interest in the case of type III intermediate filaments because most of the pathologies associated with mutations of desmin or vimentin both show IF overload (Goldfarb et al., 2008; Mohri et al., 1998; Opal and Goldman, 2013). The protein accumulation then

appears as a characteristic of type III IF related diseases: desminopathies and giant axonal neuropathy. We thus chose to work with a protein overload model and study the mechanical effect of expressing wild-type (WT) or mutated desmin on top of the endogenous WT desmin. We used a set of 3 complementary tools to characterize the mechanical properties of myoblasts in multiple cellular compartments: the whole cell, the cortex and the cytoplasm. Whole cell rheology is characterized with a parallel plate single cell rheometer, while local mechanical properties of cells are determined with micron-sized beads actuated by optical and magnetic tweezers. The association of these local and global measurements shows that while desmin has little impact on the cortex, it is a major determinant of the rheological properties of the cytoplasm, since the overall stiffness of the cells correlates with the amount of functional desmin. Indeed, the incorporation of overexpressed WT or E413K desmin into the endogenous desmin network results in cell stiffening. Strikingly, when the overexpression of the E413K mutated protein leads to the collapse of the desmin network into aggregates, a softening is observed.

RESULTS

We characterized the influence of WT or mutated desmin expression on the mechanical properties of myoblasts with a similar genetic background, C2C12 cells. Those myoblasts were electroporated with constructs leading to the expression of two forms of GFP-tagged desmin. The control experiments were performed with non-electroporated C2C12 cells (C2C12-NE). Then, the effect of over-expressing WT desmin was assessed in C2C12 expressing wild-type desmin fused with GFP (C2C12-WT-GFP). Finally, we characterized C2C12 cells expressing mutated desmin carrying the E413K mutation, fused with GFP (C2C12-E413K-GFP). The cells expressing exogenous desmin were directly selected under microscope by looking at the GFP fluorescence.

Exogenous and endogenous desmin are expressed in comparable amounts in electroporated myoblasts

Expression profiles of endogenous and exogenous desmins as well as of vimentin were quantified by Western blot analysis on at least three independent WB, using GAPDH expression level as a reference (Fig. 1.A). The expression of exogenous desmin did not disturb the expression of endogenous desmin: C2C12-WT-GFP and C2C12-E413K-GFP cells express as much endogenous desmin as C2C12-NE (Charrier et al., 2016). Furthermore, both C2C12-WT-GFP and C2C12-E413K-GFP cells express exogenous and endogenous desmin in comparable amounts: about 2 molecules of exogenous desmin per

endogenous desmin (Charrier et al., 2016). Finally, we investigated whether desmin overexpression could alter the expression of vimentin and/or actin, which both play a role cell mechanics. Using GAPDH as a reference, we measured that neither the actin expression level nor the one of vimentin were disturbed in C2C12-WT-GFP and C2C12-E413K-GFP myoblasts as compared to C2C12-NE myoblasts (Charrier et al., 2016).

The E413K mutation of desmin disturbs the exogenous desmin assembly and its incorporation into the network

To investigate the effects of exogenous desmin expression in C2C12 myoblasts, we characterized the desmin networks of the three cell types described above by confocal microscopy (Fig. 1.B and C.). The desmin network of C2C12-NE cells was stained by immunofluorescence. For cells expressing GFP-desmin, the GFP fluorescence was directly imaged. C2C12-NE cells display a normal desmin network containing well-defined and interconnected filaments spread all over the cytoplasm with an increased density in the perinuclear area. C2C12-WT-GFP myoblasts exhibit a desmin network similar to C2C12-NE cells, despite the presence of the GFP tag in the N-terminal domain of the protein. Finally, cells expressing the mutated E413K desmin protein display two phenotypes. About 70% of the cells have a desmin network spread all over the cytoplasm and organized similarly to endogenous desmin. About 30% of the cells contain both a network and cytoplasmic aggregates of desmin. The features of this aggregation are specific to the E413K desmin mutation as previously described (Charrier et al., 2016; Chourbagi et al., 2011; Levin et al., 2010). The presence of aggregates does not correlate with a high GFP signal: some very fluorescent cells do not show aggregates while less fluorescent ones display aggregates, pointing out that the aggregation of desmin-E413K-GFP is not related to its over-expression but to its dominant negative properties. The presence of aggregates could also be attributed to exogenous stresses that have been shown to increase the aggregation rate of mutated desmin *in vitro* (Segard et al., 2013).

Magnetic tweezers deeply probe cells while optical tweezers mainly probe the cellular cortex

Cells are inhomogeneous structures; their apparent mechanical properties may depend on the specific component or compartment tested, and thus on the probed spatial scale. To perform local measurements we chose an approach based on the trapping of beads, of different sizes and functionalization, specifically attached to the cell membrane, and actuated either with optical tweezers (OT) or magnetic tweezers (MT). Even if the two setups shared similarities, they used different beads with coatings that differ in nature and density. This gave different degrees of beads embedment in the cells and hence allowed to probe

different cellular compartments. This is illustrated by confocal microscopy z-stack images of C2C12 cells linked to OT and MT beads (Figure 2). The degree of embedment of beads in the cells was measured from these types of images. The beads used for OT experiments were coated with a low density of a polypeptide containing the RGD sequence (see materials and methods) and were weakly embedded into the cells, with an average embedment angle θ (as defined on Fig. 7) of 40°, corresponding to a penetration depth of 0.4 μm into the cell. As a consequence RGD-coated beads actuated with OT mainly probed the cell cortex. On the contrary, beads coated with a high level of fibronectin (see materials and methods) are deeply embedded into the cells, their average embedment angle is 110°, corresponding to a penetration depth into the cells of 3 μm on average: these beads probe both the cell cortex and the cytoplasm, similar to the single cell rheometer. The level of force necessary to move these beads largely embedded in cells could not be reached with the OT set-up and was applied with MT. We also observe that RGD coated beads do not perturb the desmin network because they are located above it (see Fig. 2.B), while fibronectin coated beads are embedded deeply enough in the cell to change the morphology of the desmin network (see Fig 2.C).

Cell creep function measurements with rheometers

The creep function of whole cells was measured with a custom-designed single cell rheometer (see Material and methods). A step stretching stress σ_0 was applied to a cell at time t=0 and held constant in time. The relative elongation $\varepsilon(t)$ of the cell was measured during stress application, and the creep function was assessed using the relationship: $J(t)=\varepsilon(t)/\sigma_0$.

Optical and magnetic tweezers (see Material and methods) were used to apply a constant step force F_0 on a bead with radius a specifically bound to a cell. The displacement $x(t)$ of the bead with respect to the cell is recorded during force application. The creep function of the cell can then be assessed using a linear model: $J(t) = g\, 2\pi\, a\, x(t) / F_0$, where g is a geometrical factor, which depends on the degree of immersion of the bead into the cell (Balland et al., 2006; Icard-Arcizet et al., 2008; Laurent et al., 2002), but can also depend on the shape of the cell (Kamgoué et al., 2007). The angle θ of bead embedment (see Fig. 7) was roughly estimated on transmission images and we used an approximate value of g as a function of θ (Balland et al., 2006; Icard-Arcizet et al., 2008; Laurent et al., 2002). In optical tweezers experiments, θ is equal to 40° on average, which gives $g\approx0.13$; in magnetic tweezers θ is equal to 110° on average and $g\approx0.56$.

Global and local cell creep functions behave as power laws of time

We characterized the myoblast mechanical properties by measuring creep functions at the scale of the whole cell, using the single cell rheometer (SCR) (Desprat et al. 2005; Desprat et al. 2006; Charrier et al., 2016) and at the local scale, using optical and magnetic tweezers (Balland et al., 2006; Icard-Arcizet et al., 2008). Examples of cell creep function measurements with the three types of rheometers are illustrated in Fig. 3. As already observed (Balland et al., 2006; Fabry et al., 2001; Icard-Arcizet et al., 2008), the displacement of the bead $x(t)$ under a constant applied force can be fitted by a power law of time, over almost three decades, typically from 0.04 s to 10 s, for all cell types. Similarly, the displacement of a bead under constant force applied by the magnetic tweezers, as well as the relative elongation of a cell under constant force applied by the SCR, are well fitted by a power law of time, over about three decades.

We fitted the local creep functions, deduced from the bead rheometers measurements, and the global creep function, measured by the SCR, as power-laws of time: $J(t) = A\, t^{\alpha}$. The parameter $1/A$ quantifies the cell rigidity while the exponent α is a characterization of energy dissipation: $\alpha=0$ would correspond to a purely elastic medium and $\alpha=1$ to a purely viscous medium. The parameters $1/A$ and α have been used to compare the mechanical properties of the three cell types characterized in this study.

For the 3 cells types and the 3 experimental techniques, the distributions of $1/A$ values are broad and approximately log-normal. This is consistent with previous measurements (Balland et al., 2006; Desprat et al., 2005; Icard-Arcizet et al., 2008). The values of α show narrower distributions, close to normal (=Gaussian) ones. Nevertheless statistical tests prove that only the distribution of α for the SRC measurements is normal. Consequently the results of the measurements for both $1/A$ and α, are displayed in terms of median values.

The global stiffness of myoblasts is correlated to the amount of functional desmin

The typical rigidity of cells, as measured with the single cell rheometer, as a function of the desmin expression is represented on Fig 4A. Non-electroporated cells and cells expressing E413K mutated desmin show similar stiffness, suggesting that adding mutated desmin to the cell does not have any effect. On the contrary, myoblasts overexpressing WT desmin through the ectopic expression of desmin-WT-GFP are significantly stiffer than the two other kinds of cells. This difference is reflected in the median values of $1/A$: about 250 Pa for C2C12-NE and C2C12-E413K and about 380 Pa for C2C12-WT-GFP. This result highlights that increasing the amount of functional desmin globally stiffens cells, by a factor of about 1.6, while adding E413K mutated desmin in myoblasts has, at first glance, no significant effect.

Mutated desmin can be polymerized into networks and at least partially integrated into the endogenous desmin network. However, in 30% of cells, part of the mutated desmin is located in aggregates, as illustrated in Fig. 1C and in [Charrier et al 2016]. To verify if the organization of the desmin in network or aggregates affects myoblast stiffness, cells expressing E413K-GFP-desmin are separated in two subgroups: cells containing cytoplasmic desmin aggregates (E413K-GFP+) and those without aggregates (E413K-GFP-). Indeed, the two subgroups show different rigidities (see Fig. 4B). The cells overexpressing desmin, with all the mutated protein engaged in network, are stiffer than non-electroporated cells, with a median value of $1/A$ at about 380 Pa, just like the desmin-WT-GFP myoblasts. On the contrary, cells containing aggregates rich in desmin are softer, with a median value of $1/A$ at about 145 Pa. In order to test a possible correlation between desmin network reinforcement and cell stiffness increase, desmin-GFP was imaged in individual cells during mechanical measurements. We then divided the C2C12-WT-GFP data in two subgroups, depending on the GFP fluorescence intensity level, which is correlated to the amount of desmin-WT-GFP expressed by the cells: cells with a low to medium fluorescence intensity ("C2C12-WT-GFP low") and cells with a high fluorescence intensity ("C2C12-WT-GFP high"). Indeed cells of the second subgroup tends to be stiffer than those of the first subgroup, but the difference is below significance (p=0.23): median value of $1/A$ of about 455 Pa *vs* about 345 Pa (see Fig. 4B). Taken together, these observations lead to the conclusion that reinforcing the desmin network with normal or mutated desmin leads to a stiffening of the cells, while collapsing the network into aggregates, which contain both endogenous and exogenous desmin, as illustrated in [Charrier et al 2016], weakens it and consequently softens the cells.

Magnetic tweezers were used as a second way to characterize cell rheology. The superparamagnetic beads used for magnetic tweezer experiments are coated with fibronectin and are deeply embedded in the cells (see Fig. 2), consequently probing the mechanical properties of different components of the cells, including, in particular, the cortex and cytoplasm. The local rigidities, as measured with magnetic tweezers, of non-electroporated cells and of cells expressing E413K mutated desmin are similar with a median value at about 87n Pa (see Fig. 4C). Nevertheless, E413K-GFP cells containing cytoplasmic desmin aggregates (E413K-GFP +) appear to be softer, with a median value of $1/A$ of at about 74 Pa and those without aggregates or with only a few of them (E413K-GFP -) appear to be stiffer, with a mean $1/A$ at about 124 Pa, although the difference is a little below the conventional significance limit (p=0.09). On the contrary, cells overexpressing desmin-WT-GFP are stiffer than NE cells, with a median value of $1/A$ at about 170 Pa (see Fig. 4C). These results are similar to those obtained with the single cell rheometer (Fig. 4B). Thus, reinforcing the desmin network by the expression of WT or mutated desmin

increases the local rigidity of cells as measured with magnetic tweezers, while collapsing it in desmin aggregates decreases the local rigidity.

Desmin does not participate to cell cortex rigidity: optical tweezers measurements.

Optical tweezers were used to probe the cortical rheology of cells with 3.47µm diameter beads linked to the membrane integrins *via* RGD peptides (Icard-Arcizet et al., 2008; Laurent et al., 2002): we used a low amount of RGD peptide coating, that was sufficient to bind cellular integrins but does not fully activate them, leading to a low degree of bead embedment in the cells. Measurements of local rheological properties of cells lead to wide distributions of *1/A* for the three cells types (Fig. 4D). The 3 populations of C2C12 share similar rigidities *1/A*, with similar median values, between 60 and 80 Pa. Thus the mechanical properties of the cellular cortex, as locally probed with optical tweezers, are not affected by the overexpression of desmin-WT-GFP or desmin-E413K-GFP in C2C12 myoblasts. The modification of the quantity and/or the quality of the desmin in myoblasts has no significant effect on the cortical rheology.

Desmin is a modulator of cytoplasm stiffness

Taken together, these results indicate that desmin has no influence on the mechanical properties of the cell cortex. This was expected, as the cortex structure is mainly composed of actin and actin binding proteins, and desmin is excluded from it (see Fig 1), although in some cell types a subplasmalemmal intermediate filament network has been identified (Quinlan et al., 2017) . However, when myoblasts overexpress functional or mutated desmin that is polymerized into networks, we show an increase in global and local stiffness as measured with the single cell rheometer and the magnetic tweezers. This most probably originates from cytoplasmic stiffening due to desmin overexpression. Strikingly, in some cells, the expression of E413K mutated desmin induces the formation of aggregates rich in desmin and cells then appear softer, presumably because part of the endogenous desmin is trapped in aggregates, which consequently weakens the IF network.

The actin cortex is more dissipative than other cell compartments probed here

The exponent α of the power-law creep function quantifies mechanical energy dissipation in the cells. In the time range which is probed here (20 ms to 20 s), the activity of motors associated with actin filaments and microtubules brings a major contribution to this dissipation (Balland et al., 2005; Robert et al., 2010). We find that α displays distinct values in function of the cellular compartments probed, as detailed in Fig. 5. For optical tweezers measurements, α is associated to the actin cortex and has similar values for

the 3 cell types, with a median value of about 0.30. The values of α measured with the single cell rheometer characterize the overall mechanical properties of cells since cortical and bulk networks are deformed and probed simultaneously. These values are overall smaller than for optical tweezers measurements, suggesting that the cell cortex is more dissipative than the rest of the cell structure. For the local magnetic tweezers measurements on beads deeply imbedded in the cell structure, the measured power-law exponent α is overall smaller than for the two other techniques, showing a relative importance in these measurements of less dissipative cellular elements, including the bulk desmin network.

In line with the previous remarks, the values of α as measured with magnetic tweezers and the single cell rheometer, i.e. techniques sensitive to bulk cell-structure properties, are slightly shifted towards small values (from 0.20 mean value to 0.18) for cells over-expressing WT desmin and E413K desmin in the absence of aggregates (Fig. 5), which is consistent with a reinforcement of the desmin network and the increase of $1/A$ (stiffness) in the same conditions. Conversely, in the presence of aggregates α values increase (from 0.20 mean value to 0.29), which is consistent with a weakening of the desmin network, associated with a cell softening. The difference in the distributions of α values for C2C12-E413K-GFP with or without aggregates is below significance (p=0.10).

Comparing the measurements from 3 techniques highlights that the value of α is higher when the cell cortex mechanics dominates the measurement (OT). For techniques sensitive to bulk cellular structure (MT and SCR), α is lower when a greater amount of functional desmin is present, and higher when the desmin network is partly collapsed. Taken together, these results suggest that the actin cortex is characterized by a higher dissipation than the desmin network.

DISCUSSION

In this study, we expressed two kinds of desmin-GFP in C2C12 myoblasts to test the hypothesis that desmin is a determinant of cell mechanical properties, which we assessed by measuring the creep function of the cells by three complementary techniques. The measurements performed by these three techniques show significantly different results. First the values of the power-law exponent α and of the typical stiffness $1/A$ are more dispersed when measured with optical and magnetic tweezers than with the single cell rheometer. Indeed, while all three techniques are sensitive to cell-to-cell variability, the bead rheometers, probing the cell at a local scale, are also sensitive to mechanical inhomogeneities within a given cell. On the other hand, the single cell rheometer probes the mechanical properties at the scale of the whole cell, thus averaging cell's internal inhomogeneities. Nevertheless within a given population of cells, the largest values of measured global stiffness are about 30 times higher than the ones measured

for the softest cells. For a single cell, the local stiffness as measured with magnetic tweezers can vary of about 100 times. The cell-to-cell disparity is almost as high as the individual cell's internal inhomogeneities.

Desmin overexpression does not have the same influence on the typical stiffness $1/A$ of the cells as measured by the 3 techniques. The optical tweezers measurements, mostly probing the cellular cortex, are insensitive to the overexpression of desmin, whereas both magnetic tweezers and single cell rheometer measurements demonstrate an overall stiffening of the cells overexpressing desmin and incorporating it into the endogenous network. We notice that the overexpression of functional desmin has little impact on the rigidity of the cortex but stiffens the inside of the cell, while the perturbation of the desmin network by a mutated desmin softens it. These results supports the idea that cell mechanics is determined by the interplay of the different cytoskeleton networks (Huber et al., 2015). They are consistent with the results obtained for vimentin in fibroblasts (Guo et al., 2013; Plodinec et al., 2011; Wang and Stamenović, 2000): it was shown that the lack of vimentin expression plays no role on the rigidity of the cortex of fibroblasts, as measured *via* micron-sized beads (Guo et al., 2013; Wang and Stamenović, 2000), while it decreases the rigidity of the cytoplasm by a factor of 2 (Guo et al., 2013; Plodinec et al., 2011). Our results, showing a stiffening of cells when desmin is over-expressed, are also consistent with recent results on cells overexpressing the desmin D399Y mutant (Even et al., 2017) and with the work published on primary human myoblasts from patients with desminopathies (R350P mutation), which appear stiffer than healthy ones (Bonakdar et al., 2012).

Using finite element calculations analogous to those described in (Mijailovich et al., 2002), with a cortex thickness $e \approx 200$nm (Clark et al., 2013), we infer from optical tweezers measurements a characteristic rigidity for the cell cortex $E^{cortex} = 1/A^{cortex} \approx 3$ kPa. It has to be underlined that this value is very sensitive to the embedment of the bead in the cell and to its distance to the coverslip. On the other hand, the rigidity as measured with the single cell rheometer is an overall rigidity which can be simply modeled as: $E^{overall} \approx E^{cortex}\, 2e/R + E^{interior}$, where R is the cell radius as defined in Fig. 6 and $E^{interior}$ is the effective stiffness of the cytoplasm and nucleus. With the results of SCR measurements, using $E^{cortex} \approx 3$kPa, $e = 200$nm and $\langle R \rangle \approx 10$µm, we find $E^{interior} \approx 120$Pa for C2-C12-NE and C2C12-E413K-GFP cells and $E^{interior} \approx 250$Pa for C2C12-WT-GFP. These values are consistent with previous estimates from SCR measurements (Monteiro et al., 2011). The order of magnitude of E^{cortex} as characterized with the optical tweezers is consistent with previous measurements (Guo et al., 2013; Robert et al., 2010; Salbreux et al., 2012). On the other hand we measure $E^{interior}$ of the order of 100 Pa, while the expected order of magnitude for the stiffness of the cytoplasm is a few to a few tens of Pa (Guo et al., 2013; Mandal et al., 2016; Robert et

al., 2010; Wirtz, 2009). We thus conclude that the nucleus probably plays a role in the measured stiffness of the interior of the cell, and that the over-expression of functional desmin could increase the value of $E^{interior}$ both by increasing the rigidity of the cytoplasm and by reinforcing the linkage between the nucleus and the other filaments of the cytoskeleton (Huber et al., 2015; Leduc and Etienne-Manneville, 2017).

The values of the power-law exponent α, which characterizes the dissipation of energy within the mechanical structure, also differs in the three kinds of measurements. This is once again consistent with the fact that the different techniques we used probe different mechanical elements of the cell. The optical tweezers based rheometer mainly probes the actin cortical skeleton, a structure that is dissipative because it is associated with myosin molecular motors. Indeed the optical tweezers rheometer measures higher values of α than the magnetic tweezers and the single cell rheometers, which also probe apparently less dissipative structures, including intermediate filaments and the nucleus. Indeed, we expect little contribution of desmin to energy dissipation in our measurements since the time range probed here (20 ms to 20 s) is shorter than the characteristic times for the dynamic of intermediate filaments networks (Leduc and Etienne-Manneville, 2017; Robert et al., 2016). Consistently increasing the amount of functional desmin also decreases the values of α, while partial depletion of the desmin network by aggregates increases it. Our results are also consistent with results on the role of vimentin in fibroblasts (Guo et al., 2013; Plodinec et al., 2011): it was noticed that decreasing the amount of vimentin enhances intracellular fluctuating movement, or in other words, the rate of energy dissipation.

CONCLUSION

In this study we characterized the contribution of desmin intermediate filaments to the overall rheology of myoblasts as well as that of their cortex. The modification of the amount of desmin or its ability to incorporate in the endogenous network has little influence on the cortical mechanical properties of cells; indeed there is no desmin to be found in this region of the cell. When the overall mechanical properties of the cell are probed (i.e. including that of the cytoplasm), cells become stiffer and less dissipative when the amount of functional desmin, whether wild-type or mutant, is increased. Conversely, when mutant desmin is non-functional, leading to formation of aggregates trapping desmin and partially depleting the desmin network, cells are softer and more dissipative. These results highlight the role of desmin intermediate filaments as a determinant of the cell cytoplasm mechanics and the way desmin mutation could soften myoblasts.

MATERIALS AND METHODS

Plasmids

A cDNA of the complete sequence of human wild-type desmin was cloned in a pEGFP-C1 vector with EcoRI-XbaI restriction sites. A single nucleotide mutation was introduced in this sequence using QuickChange II Site-Directed Mutagenesis Kit (Agilent New Technologies) according to the manufacturer's instructions. *In cellulo*, this plasmid produced the protein carrying the E413K mutation. These constructs named pEGFP-des-WT and pEGFP-Des-mut allowed production of wild-type (WT) and E413K mutated desmin fused with a GFP tag in the N-terminus. All desmin sequences were verified by sequencing (Eurofins, MWG).

Cell line, culture and electroporation

C2C12 cells (ATCC) were maintained in Dulbecco's modified Eagle's Medium (DMEM, Life Technologies) containing 10% fetal bovine serum (FBS, PAA) and 1% penicillin/streptomycin (P/S, Life Technologies). The expression of exogenous desmin in C2C12 cells was induced by electroporation of the pEGFP constructs in the cells with a Gene Pulser II (BioRad). Cells were trypsinized (Trypsin-EDTA, Life Technologies) 5 min at 37°C and resuspended in complete DMEM medium at a concentration of 2.10^6 cells/mL. Then, 400µL of the cell suspension were introduced in a Gene Pulser Cuvette 0.4cm (BioRad) with 20 µg of plasmid DNA and submitted to 250V, 1mF for approximately 25 ms. After electroporation, cells were plated for 24h on glass coverslips (VWR international) for confocal microscopy, optical and magnetic tweezers experiments. For single cell rheometer experiments, cells were plated in regular culture dishes. Then, 24h after electroporation, cells were trypsinized using trypsin-EDTA, resuspended in medium and left under weak agitation for 2h before experiments. All the experiments were performed in DMEM medium without phenol red (Life Technologies) supplemented with 10% FBS, 1% S/P and 0.15% HEPES.

Western blotting

24 h after electroporation, cells were washed three times in PBS and proteins were extracted with RIPA buffer (50 mM Tris, 150 mM NaCl, 1% NP40, 5 mM EDTA, 1 mM NA_3VO_4, 10 mM NaF, PMSF 1 mM, and antiprotease mix from Sigma-Aldrich). Then, proteins were separated by sodium dodecyl sulfate polyacrylamide gel electrophoresis (SDS-PAGE) electrophoresis on a 10% acrylamid-bisacrylamide gel and transferred to 0.2µm nitrocellulose membranes (Macherey Nagel, Duren, Germany). Membranes were saturated with 5% milk in PBS-0.5% Tween. Primary antibodies were added: Rabbit polyclonal anti-desmin (Sigma-Aldrich) at 1:1000, mouse monoclonal anti-alpha-actin

(clone 4, Merck Millipore, Darmstadt, Germany) at 1:2000, rabbit monoclonal anti-vimentin at 1:5000 (AbCam), rabbit polyclonal anti-glyceraldehyde-3-phosphate dehydrogenase (GAPDH) (Sigma-Aldrich) at 1:15000, or rabbit polyclonal anti-GFP (Life Technologies) at 1:3000. Isotype-specific secondary antibodies coupled with a horseradish peroxydase (Life Technologies) were then added at 1:10000 and revealed by incubating the membrane with enhanced chemiluminescence (Clarity, Biorad). A charge-coupled device camera FUJI Las 4000 (GE Healthcare, Little Chalfont, UK) was used to take pictures of the membrane.

Immunostaining and confocal microscopy

24h after electroporation cells were fixed with 4% paraformaldehyde (Affymetrix) for 15min at room temperature and permeabilized 10 min with 0.5% Triton X-100 in PBS. Nuclei were stained with Hoechst at 1µg/mL (Sigma-Aldrich) for 15 min at room temperature (RT). Actin was stained with phalloidin coupled to Alexa fluor 647 (Life Technologies) at 1/250 for 45 min at RT. Images of cells were taken with an inverted microscope (DM IRB, 100X oil immersion objective, 1.25 NA; Leica, Wetzlar, Germany) or a scanning and a spinning disk confocal microscopes (respectively ZEISS LSM700, 63X oil immersion objective, 1.4 NA, and Andor Revolution XD on Olympus IX81 microscope, 60X oil immersion objective, 1.42 NA). Z-stack images of myoblasts were performed with a spacing of 0.25µm between slices and 3D visualization of cells was performed using the "volume viewer" plugin of ImageJ.

Single cell rheometer

Mechanical properties at the scale of a whole single cell were characterized with a custom-made uniaxial rheometer described elsewhere in details (Desprat et al., 2005, 2006). Briefly, cells were suspended with trypsin from the culture dish, centrifuged at 1000 RPM for 5 min, and re-suspended in complete DMEM supplemented with 15mM HEPES. Regeneration of adhesion proteins at the cell surface was ensured by maintaining cells under smooth agitation for 2 h at 37°C. Cells were added in the experimental chamber filled with complete DMEM supplemented with 15mM Hepes. Then a cell was caught between the two parallel glass microplates previously coated with fibronectin 5 µg/mL, as depicted in Fig. 6. One microplate was infinitely stiff as compared to the cell, whereas the other had a calibrated stiffness *k,* comparable to cell stiffness. Before starting measurements, the cell was held 2 to 3 min between the plates to allow spreading and adhesion. Then, a controlled deflection δ was applied to the flexible microplate and held constant in time with a feedback loop. Thus a controlled constant stretching force ($F = k\delta$) was applied to the cell. The constant applied stress was calculated as $\sigma_0 = F/S = k\delta/(\pi R^2)$, where

R is the apparent contact radius between the cell and the plates, measured from bright field images, assuming that cell contacts with microplates are circular (see Fig. 6). The cell strain $\varepsilon(t)$ was directly calculated from the difference between the cell lengths $L(t)$ at time t and L_0 at time t=0, as $\varepsilon(t) = (L(t)-L_0) / L_0$. The creep function of the whole cell was assessed using the relationship: $J(t)=\varepsilon(t)/\sigma_0$. All experiments were performed in a low deformation regime ($\varepsilon<10\%$).

Optical tweezers

Micron-sized beads trapped in optical tweezers were used as handles to locally apply a controlled mechanical stress to cells. The experimental set-up is described elsewhere in details (Icard-Arcizet et al., 2008). Briefly, carboxylated silica beads 3.47 µm in diameter (Bangs Laboratories, Fishers) were functionalized with a polypeptide containing the RGD (Arg-Gly-Asp) sequence (PepTide 2000; Telios Pharmaceuticals), according to the manufacturer's procedure, to specifically bind integrin receptors at the cell membrane. The beads were incubated with cells 30 minutes before the experiment (1 to 3 beads/cell). A bead bound to a cell was trapped in an optical trap created by a 1064 nm Nd:YAG laser (Spectra Physics, Mountain View, CA) and focused through the objective of an inverted microscope (DM IRB, oil immersion objective, 1.25 NA; Leica, Wetzlar, Germany). A force F_0, ranging from 20 to 50 pN, was applied to the bead at time t=0 and maintained constant over time by keeping the bead at a fixed position with respect to the trap with a feedback loop. The relative bead-cell displacement $x(t)$ under constant applied force was then recorded. This displacement was kept less than 0.5µm to ensure linearity (Mijailovich et al., 2002).

Magnetic tweezers

Similarly, we used superparamagnetic beads actuated by a custom-designed magnetic tweezers device to assess the local mechanical properties of cells. The magnetic tweezers are built on a soft iron cylindrical rod of 5.3 mm in diameter and 52 mm in length, holding a 66 mm long solenoid consisting of about 800 turns on 8 layers of 0.5 mm copper wire on an aluminum frame enclosing the iron rod. The solenoid is connected to a custom-built current source, which can generate a current of up to 2 A. One end of the iron rod is tapered with a sharp tip (60° total angle and about 20 µm curvature radius). This set-up produces a magnetic field with both a high intensity and a high gradient. Superparamagnetic beads were 4.5 µm in diameter (Dynabeads, Invitrogen) and were coated with 5 µg/mL bovine fibronectin for 30 min at 37°C, and then saturated with BSA 10 µg/mL for 30 min at 37°C. Before an experiment, beads were incubated 30 min with cells (1 to 3 beads/cell). The experimental chamber was then mounted on

the stage of a microscope and the magnetic tweezers were attached to a micromanipulator (Eppendorf InjectMan NI-2, AG, Hamburg, Germany). The tip of the tweezers was precisely positioned 700 μm from a bead linked to a cell (see Fig. 7, accuracy about 50 nm). Finally, at time t=0, the superparamagnetic bead was submitted to a step force F_0 by establishing a step current in the solenoid. The response time of the electrical circuit is less than 20 ms. The amplitude of the force depends on the intensity in the coil and on the distance between bead and tip. We pre-calibrated it by measuring the velocity of the same beads moving in a viscous fluid (Kollmannberger 2007). It lies between 50 and 200 pN in the present experiments. The relative bead-cell displacement $x(t)$ under constant applied force was measured on the images. This displacement was kept less than 0.5 μm to ensure linearity (Mijailovich et al., 2002). The power supply and the camera were controlled and synchronized by computer, using the MicroManager software.

Statistics

Gaussian distributions of the measured values were tested using the Shapiro-Wilk method. Since most values did not exhibit normal (Gaussian) distributions, a non-parametric (Kruskal-Wallis) test was applied to the data, with a statistically significant p-value ≤ 0.05.

AUTHORS CONTRIBUTION

E.C. and L.M. designed research, performed research, analyzed data, and wrote the paper. F.D. performed experiments. A.A., P.V., F.G., S.B.-P. and S.H. designed research, analyzed data, and wrote the paper.

ACKNOWLEDGEMENTS

This work has been funded by grants from Association Française contre les myopathies (AFM 15454); Agence Nationale de la Recherche (ANR-13-BSV5-0017); and Labex Who Am I? (Transition postdoctoral program). The authors are grateful to Katrina Cruz for proof reading the manuscript.

LIST OF ABREVIATIONS

DMEM: Dulbecco's Modified Eagle's Medium
FBS: Fetal Bovine Serum
MT: Magnetic Tweezers
OT: Optical Tweezers
SRC: Single Cell Rheometer
WT: Wild-Type

REFERENCES

Alam, H., Sehgal, L., Kundu, S.T., Dalal, S.N., Vaidya, M.M., 2011. Novel function of keratins 5 and 14 in proliferation and differentiation of stratified epithelial cells. Mol. Biol. Cell 22, 4068–4078. https://doi.org/10.1091/mbc.E10-08-0703

Asparuhova, M.B., Gelman, L., Chiquet, M., 2009. Role of the actin cytoskeleton in tuning cellular responses to external mechanical stress. Scand. J. Med. Sci. Sports 19, 490–499. https://doi.org/10.1111/j.1600-0838.2009.00928.x

Balland, M., Desprat, N., Icard, D., Féréol, S., Asnacios, A., Browaeys, J., Hénon, S., Gallet, F., 2006. Power laws in microrheology experiments on living cells: Comparative analysis and modeling. Phys. Rev. E Stat. Nonlin. Soft Matter Phys. 74, 021911.

Balland, M., Richert, A., Gallet, F., 2005. The dissipative contribution of myosin II in the cytoskeleton dynamics of myoblasts. Eur. Biophys. J. 34, 255–261. https://doi.org/10.1007/s00249-004-0447-7

Bär, H., Goudeau, B., Wälde, S., Casteras-Simon, M., Mücke, N., Shatunov, A., Goldberg, Y.P., Clarke, C., Holton, J.L., Eymard, B., Katus, H.A., Fardeau, M., Goldfarb, L., Vicart, P., Herrmann, H., 2007. Conspicuous involvement of desmin tail mutations in diverse cardiac and skeletal myopathies. Hum. Mutat. 28, 374–386. https://doi.org/10.1002/humu.20459

Blanchoin, L., Boujemaa-Paterski, R., Sykes, C., Plastino, J., 2014. Actin dynamics, architecture, and mechanics in cell motility. Physiol. Rev. 94, 235–263. https://doi.org/10.1152/physrev.00018.2013

Bonakdar, N., Luczak, J., Lautscham, L., Czonstke, M., Koch, T.M., Mainka, A., Jungbauer, T., Goldmann, W.H., Schröder, R., Fabry, B., 2012. Biomechanical characterization of a desminopathy in primary human myoblasts. Biochem. Biophys. Res. Commun. 419, 703–707. https://doi.org/10.1016/j.bbrc.2012.02.083

Charrier, E.E., Asnacios, A., Milloud, R., De Mets, R., Balland, M., Delort, F., Cardoso, O., Vicart, P., Batonnet-Pichon, S., Hénon, S., 2016. Desmin Mutation in the C-Terminal Domain Impairs Traction Force Generation in Myoblasts. Biophys. J. 110, 470–480. https://doi.org/10.1016/j.bpj.2015.11.3518

Charrier, E.E., Janmey, P.A., 2016. Mechanical Properties of Intermediate Filament Proteins. Methods Enzymol. 568, 35–57. https://doi.org/10.1016/bs.mie.2015.09.009

Chernyatina, A.A., Nicolet, S., Aebi, U., Herrmann, H., Strelkov, S.V., 2012. Atomic structure of the vimentin central α-helical domain and its implications for intermediate filament assembly. Proc. Natl. Acad. Sci. U. S. A. 109, 13620–13625. https://doi.org/10.1073/pnas.1206836109

Chourbagi, O., Bruston, F., Carinci, M., Xue, Z., Vicart, P., Paulin, D., Agbulut, O., 2011. Desmin mutations in the terminal consensus motif prevent synemin-desmin heteropolymer filament assembly. Exp. Cell Res. 317, 886–897. https://doi.org/10.1016/j.yexcr.2011.01.013

Clark, A.G., Dierkes, K., Paluch, E.K., 2013. Monitoring actin cortex thickness in live cells. Biophys. J. 105, 570–580. https://doi.org/10.1016/j.bpj.2013.05.057

Clemen, C.S., Herrmann, H., Strelkov, S.V., Schröder, R., 2013. Desminopathies: pathology and mechanisms. Acta Neuropathol. (Berl.) 125, 47–75. https://doi.org/10.1007/s00401-012-1057-6

Desprat, N., Guiroy, A., Asnacios, A., 2006. Microplates-based rheometer for a single living cell. Rev. Sci. Instrum. 77, 055111. https://doi.org/10.1063/1.2202921

Desprat, N., Richert, A., Simeon, J., Asnacios, A., 2005. Creep function of a single living cell. Biophys. J. 88, 2224–2233. https://doi.org/10.1529/biophysj.104.050278

Eckes, B., Dogic, D., Colucci-Guyon, E., Wang, N., Maniotis, A., Ingber, D., Merckling, A., Langa, F., Aumailley, M., Delouvée, A., Koteliansky, V., Babinet, C., Krieg, T., 1998. Impaired mechanical stability, migration and contractile capacity in vimentin-deficient fibroblasts. J. Cell Sci. 111 (Pt 13), 1897–1907.

Even, C., Abramovici, G., Delort, F., Rigato, A.F., Bailleux, V., de Sousa Moreira, A., Vicart, P., Rico, F., Batonnet-Pichon, S., Briki, F., 2017. Mutation in the Core Structure of Desmin Intermediate Filaments Affects Myoblast Elasticity. Biophys. J. 113, 627–636. https://doi.org/10.1016/j.bpj.2017.06.020

Fabry, B., Maksym, G.N., Butler, J.P., Glogauer, M., Navajas, D., Fredberg, J.J., 2001. Scaling the microrheology of living cells. Phys. Rev. Lett. 87, 148102.

Fuchs, E., Weber, K., 1994. Intermediate filaments: structure, dynamics, function, and disease. Annu. Rev. Biochem. 63, 345–382. https://doi.org/10.1146/annurev.bi.63.070194.002021

Goldfarb, L.G., Olive, M., Vicart, P., Goebel, H.H., 2008. Intermediate Filament Diseases: Desminopathy. Adv. Exp. Med. Biol. 642, 131–164.

Guo, M., Ehrlicher, A.J., Mahammad, S., Fabich, H., Jensen, M.H., Moore, J.R., Fredberg, J.J., Goldman, R.D., Weitz, D.A., 2013. The role of vimentin intermediate filaments in cortical and cytoplasmic mechanics. Biophys. J. 105, 1562–1568. https://doi.org/10.1016/j.bpj.2013.08.037

Huber, F., Boire, A., López, M.P., Koenderink, G.H., 2015. Cytoskeletal crosstalk: when three different personalities team up. Curr. Opin. Cell Biol. 32, 39–47. https://doi.org/10.1016/j.ceb.2014.10.005

Icard-Arcizet, D., Cardoso, O., Richert, A., Hénon, S., 2008. Cell stiffening in response to external stress is correlated to actin recruitment. Biophys. J. 94, 2906–2913. https://doi.org/10.1529/biophysj.107.118265

Ingber, D.E., 2006. Cellular mechanotransduction: putting all the pieces together again. FASEB J. Off. Publ. Fed. Am. Soc. Exp. Biol. 20, 811–827. https://doi.org/10.1096/fj.05-5424rev

Ivaska, J., Pallari, H.-M., Nevo, J., Eriksson, J.E., 2007. Novel functions of vimentin in cell adhesion, migration, and signaling. Exp. Cell Res. 313, 2050–2062. https://doi.org/10.1016/j.yexcr.2007.03.040

Kamgoué, A., Ohayon, J., Tracqui, P., 2007. Estimation of cell Young's modulus of adherent cells probed by optical and magnetic tweezers: influence of cell thickness and bead immersion. J. Biomech. Eng. 129, 523–530. https://doi.org/10.1115/1.2746374

Laurent, V.M., Hénon, S., Planus, E., Fodil, R., Balland, M., Isabey, D., Gallet, F., 2002. Assessment of mechanical properties of adherent living cells by bead micromanipulation: comparison of magnetic twisting cytometry vs optical tweezers. J. Biomech. Eng. 124, 408–421.

Leduc, C., Etienne-Manneville, S., 2017. Regulation of microtubule-associated motors drives intermediate filament network polarization. J. Cell Biol. 216, 1689–1703. https://doi.org/10.1083/jcb.201607045

Levin, J., Bulst, S., Thirion, C., Schmidt, F., Bötzel, K., Krause, S., Pertl, C., Kretzschmar, H., Walter, M.C., Giese, A., Lochmüller, H., 2010. Divergent molecular effects of desmin mutations on protein assembly in myofibrillar myopathy. J. Neuropathol. Exp. Neurol. 69, 415–424. https://doi.org/10.1097/NEN.0b013e3181d71305

Mandal, K., Asnacios, A., Goud, B., Manneville, J.-B., 2016. Mapping intracellular mechanics on micropatterned substrates. Proc. Natl. Acad. Sci. U. S. A. 113, E7159–E7168. https://doi.org/10.1073/pnas.1605112113

Mijailovich, S.M., Kojic, M., Zivkovic, M., Fabry, B., Fredberg, J.J., 2002. A finite element model of cell deformation during magnetic bead twisting. J. Appl. Physiol. 93, 1429–1436. https://doi.org/10.1152/japplphysiol.00255.2002

Mohri, I., Taniike, M., Yoshikawa, H., Higashiyama, M., Itami, S., Okada, S., 1998. A case of giant axonal neuropathy showing focal aggregation and hypophosphorylation of intermediate filaments. Brain Dev. 20, 594–597.

Monteiro, E., Yvonnet, J., He, Q.-C., Cardoso, O., Asnacios, A., 2011. Analyzing the interplay between single cell rheology and force generation through large deformation finite element models. Biomech. Model. Mechanobiol. 10, 813–830. https://doi.org/10.1007/s10237-010-0276-9

Opal, P., Goldman, R.D., 2013. Explaining intermediate filament accumulation in giant axonal neuropathy. Rare Dis. 1. https://doi.org/10.4161/rdis.25378

Plodinec, M., Loparic, M., Suetterlin, R., Herrmann, H., Aebi, U., Schoenenberger, C.-A., 2011. The nanomechanical properties of rat fibroblasts are modulated by interfering with the vimentin intermediate filament system. J. Struct. Biol. 174, 476–484. https://doi.org/10.1016/j.jsb.2011.03.011

Pruszczyk, P., Kostera-Pruszczyk, A., Shatunov, A., Goudeau, B., Dramiñska, A., Takeda, K., Sambuughin, N., Vicart, P., Strelkov, S.V., Goldfarb, L.G., Kamiñska, A., 2007. Restrictive cardiomyopathy with atrioventricular conduction block resulting from a desmin mutation. Int. J. Cardiol. 117, 244–253. https://doi.org/10.1016/j.ijcard.2006.05.019

Quinlan, R.A., Schwarz, N., Windoffer, R., Richardson, C., Hawkins, T., Broussard, J.A., Green, K.J., Leube, R.E., 2017. A rim-and-spoke hypothesis to explain the biomechanical roles for cytoplasmic intermediate filament networks. J. Cell Sci. 130, 3437–3445. https://doi.org/10.1242/jcs.202168

Robert, A., Hookway, C., Gelfand, V.I., 2016. Intermediate filament dynamics: What we can see now and why it matters. BioEssays News Rev. Mol. Cell. Dev. Biol. 38, 232–243. https://doi.org/10.1002/bies.201500142

Robert, D., Nguyen, T.-H., Gallet, F., Wilhelm, C., 2010. In vivo determination of fluctuating forces during endosome trafficking using a combination of active and passive microrheology. PloS One 5, e10046. https://doi.org/10.1371/journal.pone.0010046

Roca-Cusachs, P., Rio, A. del, Puklin-Faucher, E., Gauthier, N.C., Biais, N., Sheetz, M.P., 2013. Integrin-dependent force transmission to the extracellular matrix by α-actinin triggers adhesion maturation. Proc. Natl. Acad. Sci. 110, E1361–E1370. https://doi.org/10.1073/pnas.1220723110

Salbreux, G., Charras, G., Paluch, E., 2012. Actin cortex mechanics and cellular morphogenesis. Trends Cell Biol. 22, 536–545. https://doi.org/10.1016/j.tcb.2012.07.001

Segard, B.-D., Delort, F., Bailleux, V., Simon, S., Leccia, E., Gausseres, B., Briki, F., Vicart, P., Batonnet-Pichon, S., 2013. N-acetyl-L-cysteine prevents stress-induced desmin aggregation in cellular models of desminopathy. PloS One 8, e76361. https://doi.org/10.1371/journal.pone.0076361

Steinert, P.M., Idler, W.W., Cabral, F., Gottesman, M.M., Goldman, R.D., 1981. In vitro assembly of homopolymer and copolymer filaments from intermediate filament subunits of muscle and fibroblastic cells. Proc. Natl. Acad. Sci. U. S. A. 78, 3692–3696.

Wang, N., Stamenović, D., 2000. Contribution of intermediate filaments to cell stiffness, stiffening, and growth. Am. J. Physiol. Cell Physiol. 279, C188-194.

Wang, N., Tytell, J.D., Ingber, D.E., 2009. Mechanotransduction at a distance: mechanically coupling the extracellular matrix with the nucleus. Nat. Rev. Mol. Cell Biol. 10, 75–82. https://doi.org/10.1038/nrm2594

Weber, K., Geisler, N., 1985. Intermediate Filaments: Structural Conservation and Divergence. Ann. N. Y. Acad. Sci. 455, 126–143. https://doi.org/10.1111/j.1749-6632.1985.tb50408.x
Welch, M.D., Iwamatsu, A., Mitchison, T.J., 1997. Actin polymerization is induced by Arp2/3 protein complex at the surface of Listeria monocytogenes. Nature 385, 265–269. https://doi.org/10.1038/385265a0
Wirtz, D., 2009. Particle-tracking microrheology of living cells: principles and applications. Annu. Rev. Biophys. 38, 301–326. https://doi.org/10.1146/annurev.biophys.050708.133724

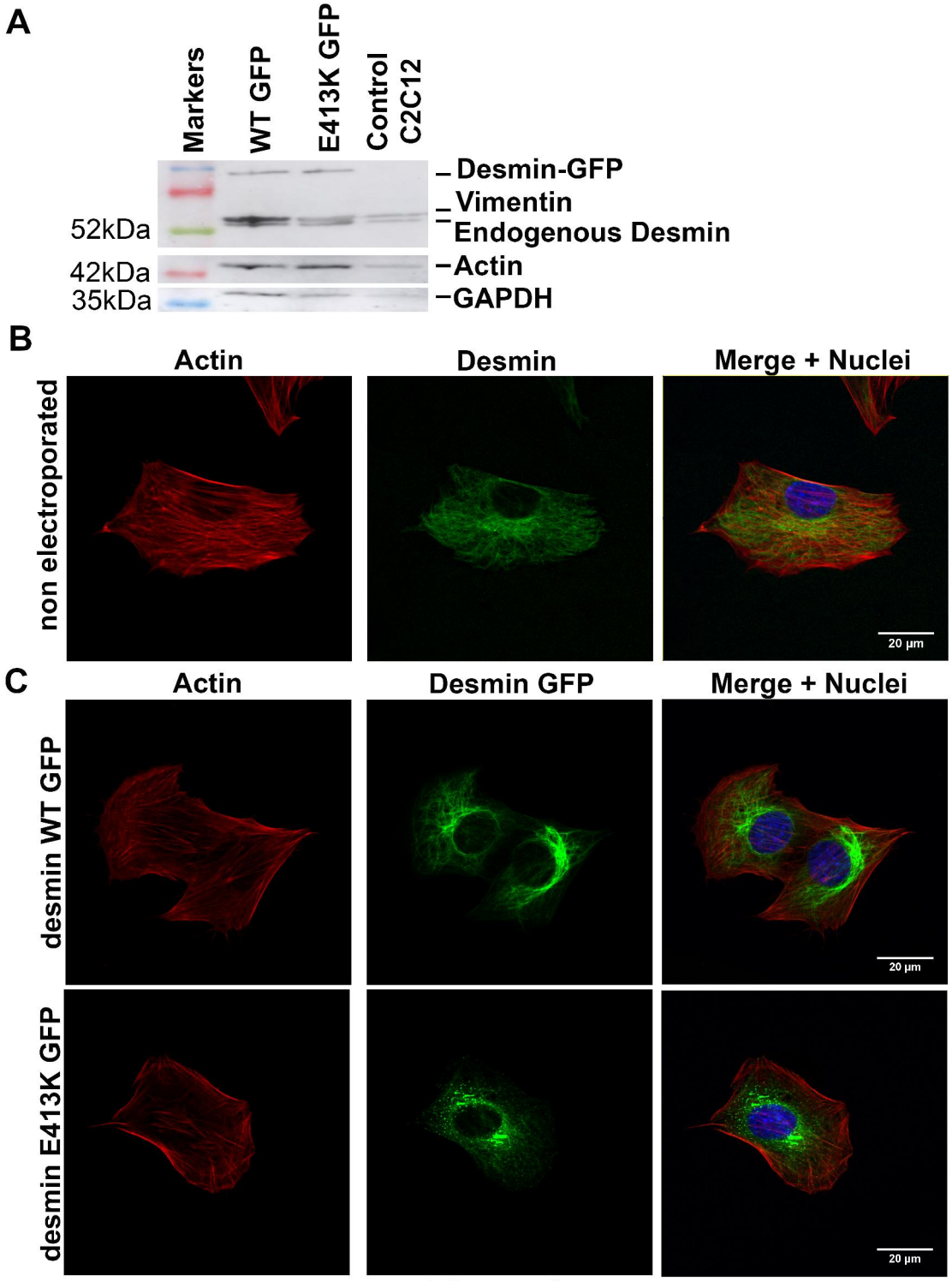
A
Markers
WT GFP
E413K GFP
Control C2C12
52kDa
42kDa
35kDa
Desmin-GFP
Vimentin
Endogenous Desmin
Actin
GAPDH
B
Actin
Desmin
Merge + Nuclei
non electroporated
20 µm
C
Actin
Desmin GFP
Merge + Nuclei
desmin WT GFP
desmin E413K GFP
20 µm
20 µm

Figure 1

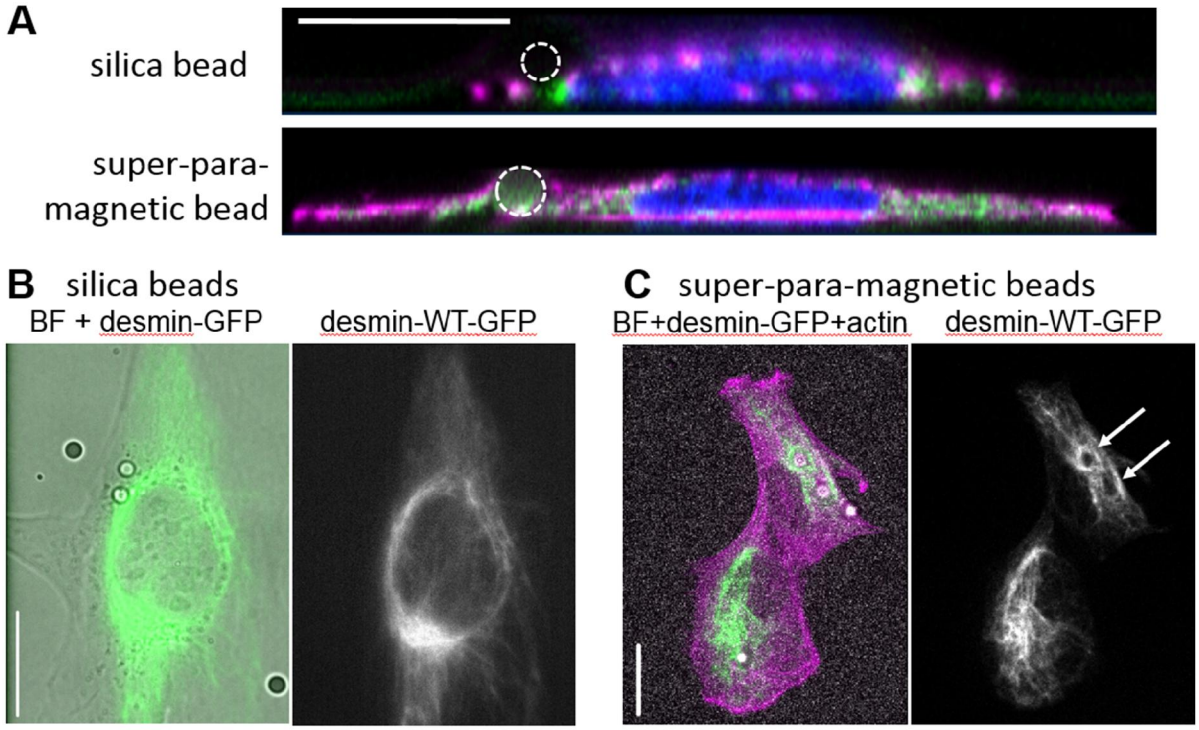

Figure 2

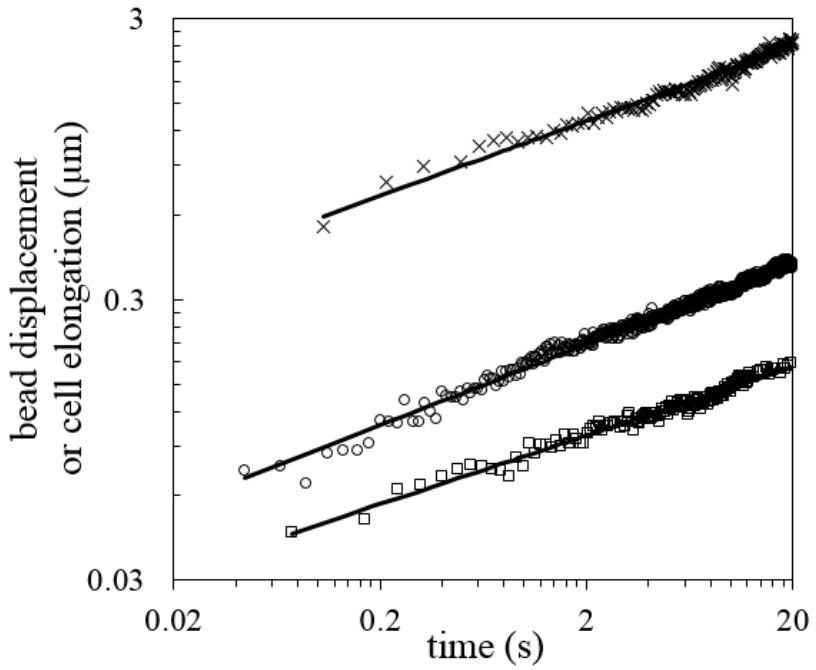

Figure 3

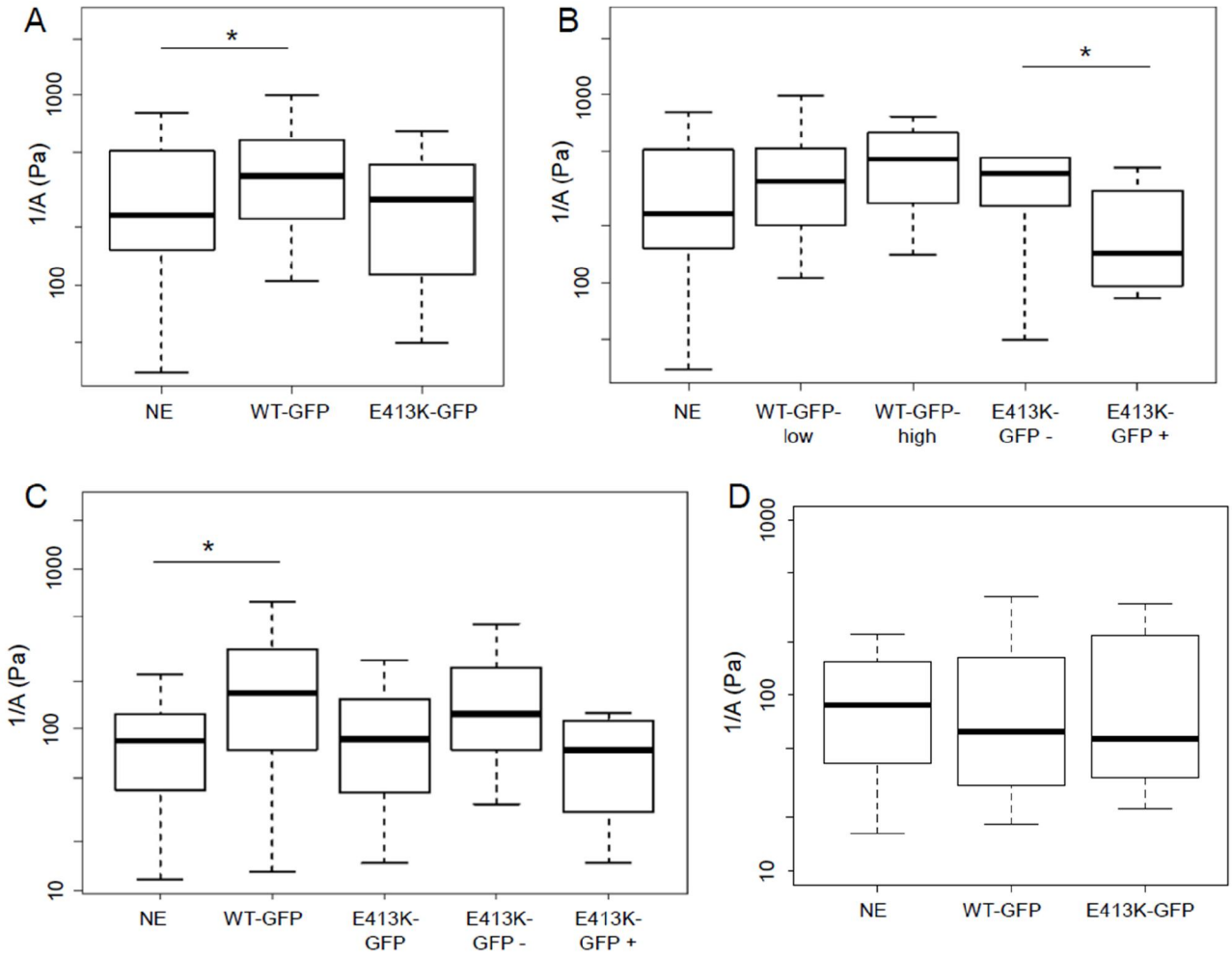
A
1/A (Pa)
1000
100
*
NE
WT-GFP
E413K-GFP
B
1/A (Pa)
1000
100
*
NE
WT-GFP-low
WT-GFP-high
E413K-GFP -
E413K-GFP +
C
1/A (Pa)
1000
100
10
*
NE
WT-GFP
E413K-GFP
E413K-GFP -
E413K-GFP +
D
1/A (Pa)
1000
100
10
NE
WT-GFP
E413K-GFP

Figure 4

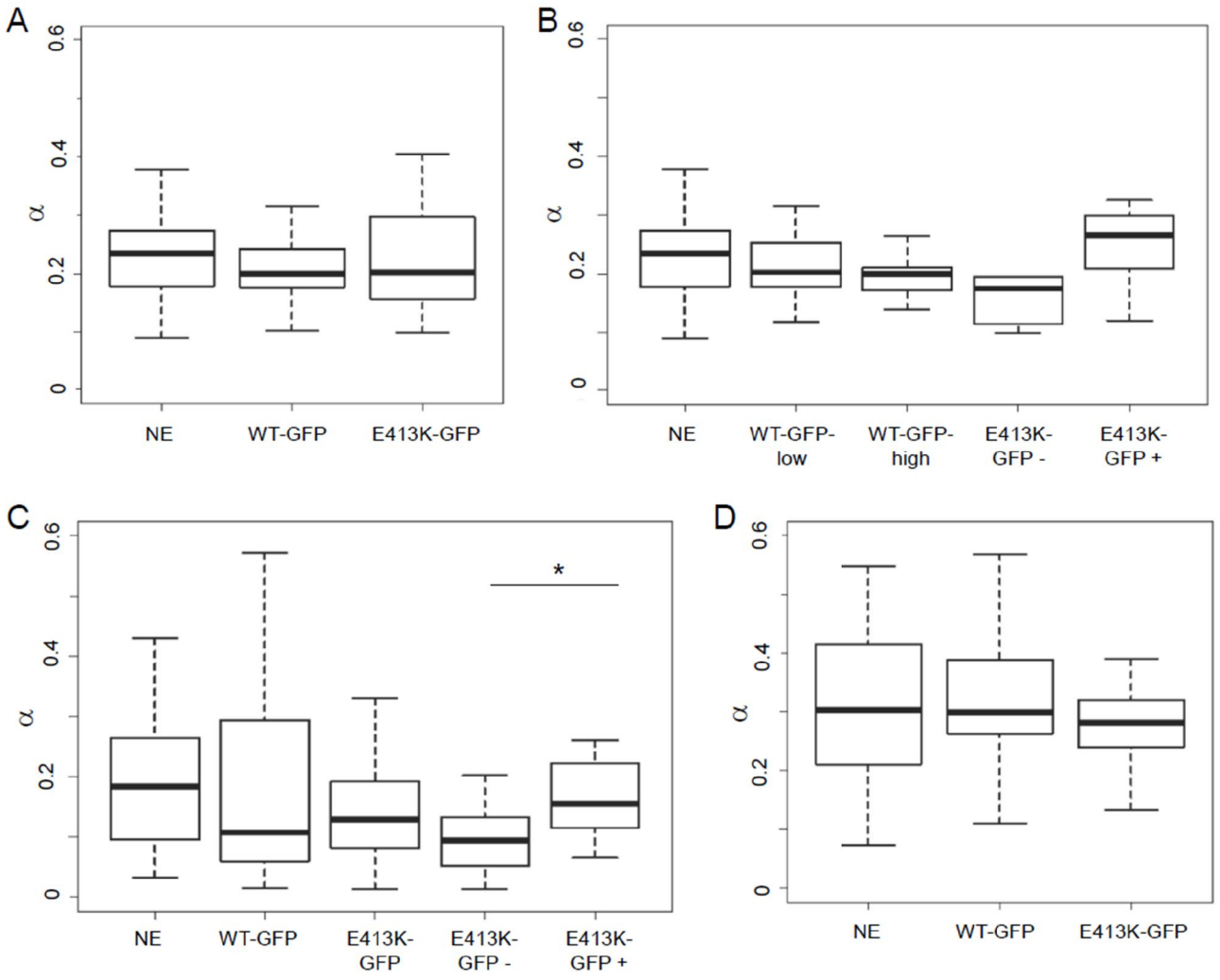
A
B
C
D
α
0
0.2
0.4
0.6
NE
WT-GFP
E413K-GFP
WT-GFP-low
WT-GFP-high
E413K-GFP -
E413K-GFP +
*

Figure 5

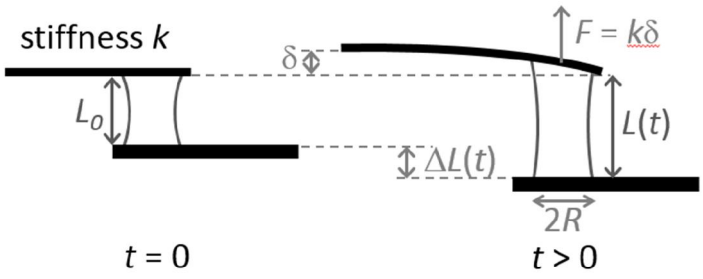

Figure 6

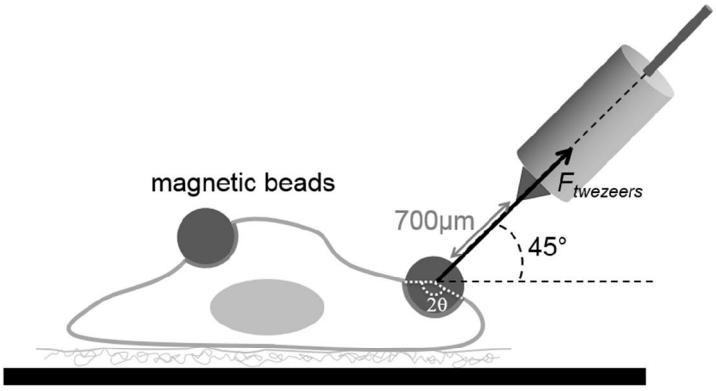

Figure 7

Figure captions

Figure 1: Impact of WT or mutated desmin-GFP expression on desmin and actin network morphologies in C2C12 myoblasts.
A: Immunoblots for analyzing desmin, actin, and vimentin expression in non-electroporated C2C12 cells (Control C2C12), C2C12 expressing WT desmin-GFP (WT GFP) or E413K mutated desmin-GFP (E413K GFP). GAPDH is used as a loading control.
B: Confocal images of actin and desmin in non electroporated C2C12 cells. Desmin was stained by immunofluorescence, actin was stained with phalloidin and nuclei with Hoechst.
Scale bar = 20 μm.
C: Confocal images of actin and desmin networks in C2C12-WT-GFP cells (desmin WT GFP) and C2C12- E413K-GFP cells (desmin E413K GFP). Exogenous desmin network was directly visualized by imaging the GFP fluorescence. C2C12-WT-GFP myoblasts exhibited normal desmin and actin network morphologies. C2C12-E413K-GFP cells displayed two phenotypes: 70% of cells contained only desmin networks, 30% of cells contained both desmin networks and cytoplasmic aggregates.
Scale bar = 20 μm.

Figure 2: Images of C2C12 myoblasts, expressing desmin-WT-GFP, linked to the two kinds of beads.
A: Z-profiles of myoblasts linked to a silica optical tweezers bead (top) or a superparamagnetic magnetic tweezers bead (bottom). Nuclei are stained in blue with Hoescht, actin is stained in magenta with phalloidin and desmin-GFP appears in green. Bead locations are designated with the white dashed circles. Silica beads are weakly embedded into cells while superparamagnetic beads are deeply embedded.
B: Bright field and epifluorescence images of myoblasts linked to silica beads. Bead has no impact on the desmin network morphology (right).
C: Bright field and fluorescence images of myoblasts linked to superparamagnetic beads. The network of desmin (right) is perturbed at the bead location: the beads indent the desmin network (white arrows).
Scale bars = 20 μm

Figure 3: Creep function measurement carried out with the different rheometers. The elongation $\Delta L(t)$ of a cell (single cell rheometer ×) or the displacement $x(t)$ of a bead (optical tweezers ○, magnetic tweezers □) under a constant applied force is plotted as a function of time in a log-log scale. $x(t)$ and $\Delta L(t)$ are well fitted by power laws of time over almost three decades.

Figure 4: Boxplots of the myoblasts characteristic rigidities $1/A$, obtained with the single cell rheometer (A and B), the magnetic tweezers (C) and the optical tweezers (D), on single non-electroporated

myoblasts (NE), myoblasts expressing desmin-WT-GFP (WT-GFP) or desmin-E413K-GFP (E413K-GFP). E413K-GFP myoblasts were separated in two subgroups: cells containing cytoplasmic desmin aggregates (E413K-GFP +) and cells without aggregates (E413K-GFP -). WT-GFP myoblasts were separated in two subgroups: cells with a high GFP-fluorescence intensity level (WT-GFP-high) and cells with a low or intermediate GFP-fluorescence intensity level (WT-GFP-low). The star symbols indicate significant *p*-values: $p = 0.02$ for the comparison between NE and WT-GFP cells in Fig. 4 A and 4 B, and $p=0.05$ for the comparison between E413K-GFP + and E413K-GFP - cells in Fig. 4 B. For the comparison between WT-GFP-high and WT-GFP-low cells in Fig. 4 B, $p=0.23$. For the comparison between E413K-GFP + and E413K-GFP - cells in Fig. 4 C, $p=0.09$.
Numbers of cells. A: 45 NE, 53 WT-GFP, 20 E413K-GFP; B: 34 WT-GFP-low, 19 WT-GFP-high, 10 E413K-GFP +, 10 E413K-GFP - ; C: 34 NE, 25 WT-GFP, 12 E413K-GFP -, 13 E413K-GFP +; C: 23 NE, 21 WT-GFP, 26 E413K-GFP.

Figure 5: Boxplots of the values of α, obtained with the same techniques and cells than described in figure 4, (A and B) single cell rheometer, (C) magnetic tweezers, (D) optical tweezers. Three cell types were studied, single non-electroporated myoblasts (NE), myoblasts expressing desmin-WT-GFP (WT-GFP) or desmin-E413K-GFP (E413K-GFP). E413K-GFP myoblasts were separated in two subgroups: cells containing cytoplasmic desmin aggregates (E413K-GFP +) and cells without aggregates (E413K-GFP -). WT-GFP myoblasts were separated in two subgroups: cells with a high GFP-fluorescence intensity level (WT-GFP-high) and cells with a low or intermediate GFP-fluorescence intensity level (WT-GFP-low). The star symbol indicates a significant *p*-value: $p = 0.04$ for the comparison between E413K-GFP+ and E413K-GFP- in Fig. 5C.
Numbers of cells. A: 45 NE, 53 WT-GFP, 20 E413K-GFP; B: 34 WT-GFP-low, 19 WT-GFP-high, 10 E413K-GFP +, 10 E413K-GFP - ; C: 34 NE, 25 WT-GFP, 12 E413K-GFP -, 13 E413K-GFP +; C: 23 NE, 21 WT-GFP, 26 E413K-GFP.

Figure 6: Principle of a creep experiment with the single cell rheometer. A cell is caught between two microplates, a flexible one (top, stiffness k) and the rigid one (bottom, much stiffer than cells). At the beginning of the experiment, the flexible microplate is displaced by a distance δ, held constant over time by a feedback loop applying a displacement $\Delta L(t)=L(t) - L_0$ to the rigid microplate. The constant applied stress is calculated from the displacement δ, while the cell strain is retrieved from its elongation $\Delta L(t)$.

Figure 7: Schematic representation of the magnetic tweezers. Superparamagnetic beads of 4.5 µm in diameter are attached to the cell through a fibronectin coating. A copper solenoid and a soft iron tip produce a high magnetic field gradient, creating a force $F_{tweezers}$ on the beads.

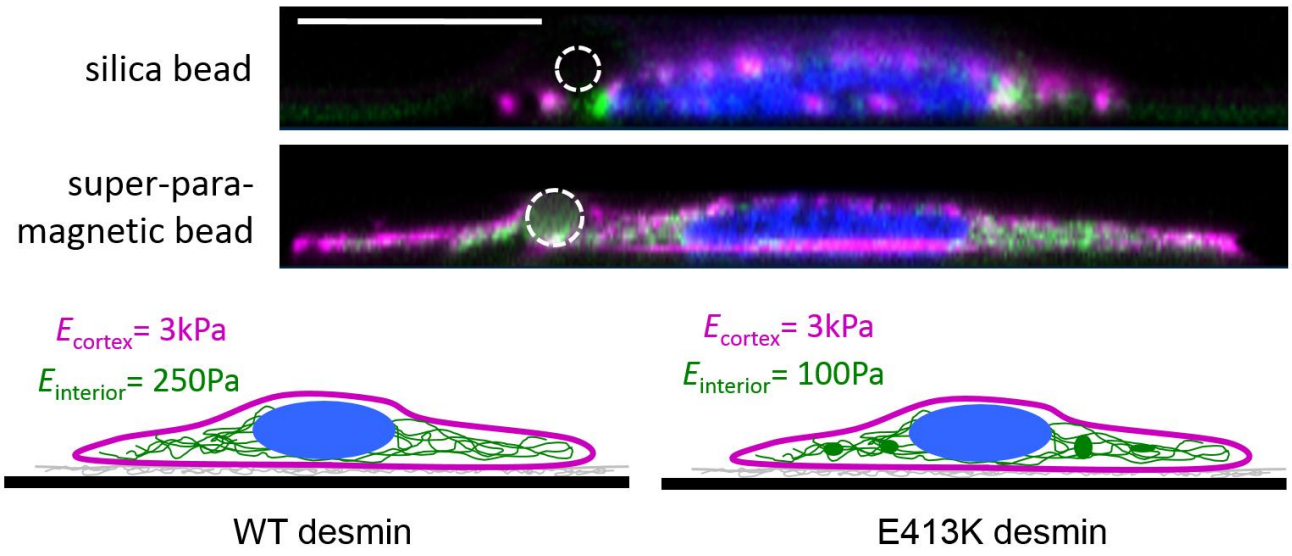

Desmin is an intermediate filament maintaining the structural integrity of the contractile apparatus in muscle cells. We demonstrate here the implication of desmin in the passive mechanical properties of immature muscle cells. Desmin plays a negligible role in the mechanical properties of the cell cortex, however the over-all rigidity of myoblasts scales with the amount of functional desmin engaged into cytoplasmic networks.